

MAGNETIC FIELD-VECTOR MEASUREMENTS IN QUIESCENT PROMINENCES VIA  
THE HANLE EFFECT: ANALYSIS OF PROMINENCES OBSERVED AT  
PIC-DU-MIDI AND AT SACRAMENTO PEAK

V. Bommier,\* J. L. Leroy,\*\* and S. Sahal-Bréchet\*

\**Observatoire de Paris-Meudon, 92190 Meudon, France*

\*\**Observatoire du Pic-du-Midi et de Toulouse, 31400 Toulouse, France*

The Hanle effect method for magnetic field vector diagnostics has now provided results on the magnetic field strength and direction in quiescent prominences, from linear polarization measurements in the He I  $D_3$  line, performed at the Pic-du-Midi and at Sacramento Peak. However, there is an inescapable ambiguity in the field vector determination: each polarization measurement provides two field vector solutions symmetrical with respect to the line-of-sight. A statistical analysis capable of solving this ambiguity has been recently applied to the large sample of prominences observed at the Pic-du-Midi (Leroy et al., 1984); the same method of analysis applied to the prominences observed at Sacramento Peak (Athay et al., 1983) provides results in agreement on the most probable magnetic structure of prominences; these results are detailed in the following paragraphs.

The Sacramento Peak spectropolarimeter has provided narrow-band polarization data, in which the two components of He I  $D_3$  are fully resolved, which form a pair of lines adequate for the achievement of the complete field vector determination (Bommier et al., 1981). In a sample of 14 prominences observed and interpreted (Athay et al., 1983), the two symmetrical field vectors have been found to approximate  $90^\circ$  starting from the local solar radius, i.e. neighbouring the horizontal plane.

Two-line observations in broad-band polarization have been recently performed with the Pic-du-Midi coronagraph polarimeter, in He I  $D_3$  and Hydrogen  $H\beta$ , which have given the same result on the field direction (Leroy, Bommier, Sahal-Bréchet, to be published). Considering that result, one-line observations previously made of the unresolved He I  $D_3$  line have been interpreted in terms of the field strength and azimuth angle only in 120 prominences of the Polar Crown (Leroy et al., 1983) and 256 prominences of medium and low latitude (Leroy et al., 1984).

In most cases, the two symmetrical field-vectors do not cross the prominence long axis in the same sense; further investigation is then required before we are able to provide observational constraints on the type of the magnetic structure of prominences, in particular with respect to the polarity of the photospheric magnetic field on each side of the neutral line underlying the prominence.

Owing to the symmetry of the two field vectors with respect to the line-of-sight, one has the following "mirror effect" within the two angles  $\alpha_V$  and  $\alpha_F$  between the field vectors and the prominence long axis, and the angle  $\beta$  between the prominence long axis and the line-of-sight (Fig. 1):

$$\alpha_V + \alpha_F = 2\beta \quad (1)$$

The precise definition of the sign and value of  $\alpha$  and  $\beta$  can be found in Leroy et al. (1984, see Fig. 4 of that paper); our convention is that positive and negative  $\alpha$  angles correspond to prominence field orientations consistent and inconsistent respectively with the potential and non-potential field orientation with respect to the polarity of the neighbouring photospheric field.

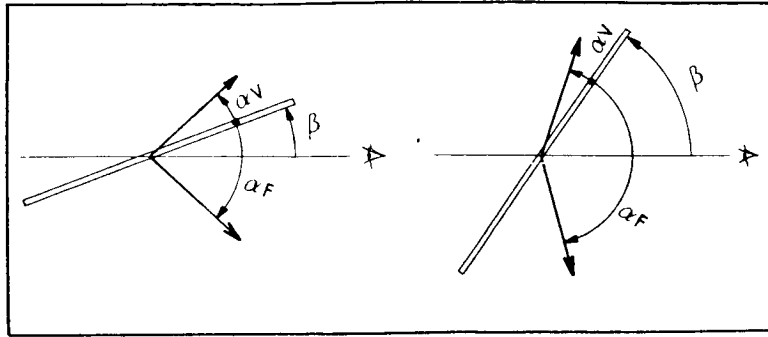


Fig. 1. The magnetic field determination through a polarimetric analysis provides two field vector solutions symmetrical with respect to the line-of-sight.

If there is a preferential value  $\alpha_c$  in the sample of prominences, one has:

$$\alpha_V = \alpha_c \quad (2)$$

then according to (1)

$$\alpha_F = -\alpha_c + 2\beta \quad (3)$$

For a couple of two observed field vectors, there is no a-priori choice of  $\alpha_F$  and  $\alpha_V$  between the two  $\alpha$  angles.

Figure 2 is a plot of relations (2) and (3) for  $\alpha_c = 30^\circ$ . The points on Fig. 2 correspond to the observed  $\alpha$  and  $\beta$  values for 12 of the 14 prominences observed at Sacramento Peak. Two prominences have been discarded, as the direction of the prominence long axis cannot be established. The values of the  $\alpha$  angles have been derived by averaging the values obtained for each measurement by Athay et al., (1983, see table 2 of that paper). In Table 1 and Fig. 2, the prominence names refer to that paper; in each prominence, the averages have been done for each day and each position angle.

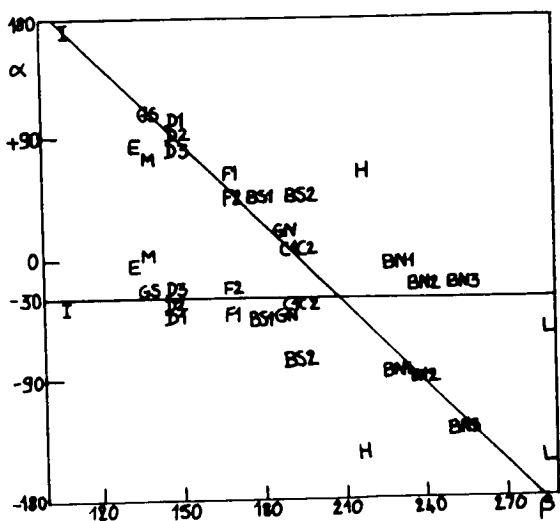


Fig. 2. Plot of relations (2) and (3) for  $\alpha_c = -30^\circ$ , and of the observed averaged values for 12 prominences observed at Sacramento Peak (Athay et al., 1983). Compare with Fig. 6 of Leroy et al. (1984).

A similar plot can be found on Fig. 6 of Leroy et al. (1984), for 120 of 256 prominences observed at Pic-du-Midi, for which the geometrical parameters and the direction of the underlying neutral line, can be established with accuracy. This sample of 120 prominences corresponds to 900 measurements.

Figure 2 represents the least-square fitting of (2) and (3) in the observed data; the squared residues  $\Sigma (0 - C)^2$  in the least-square fitting are given on Figure 3 as a function of  $\alpha_c$ , for the Pic-du-Midi data (full line, Fig. 7 of Leroy et al., 1984), and for the Sacramento Peak data (dotted line). In the fitting calculation, the data must be weighed according to their accuracy. Two kinds of data uncertainties have to be considered:

- 1) Geometrical errors, which are roughly constant over one given prominence.
- 2) Photometric errors which can occur on each measurement.

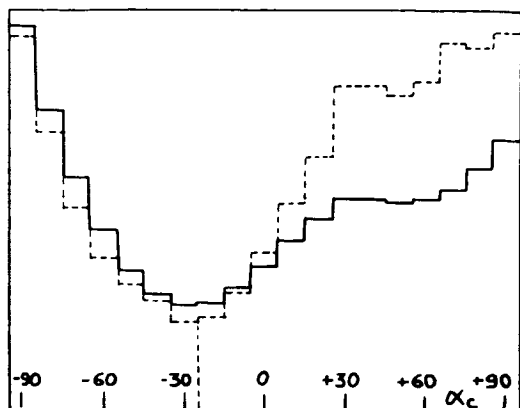


Fig. 3. The squared residues in the least-squares fitting of relations (2) and (3) in the Pic-du-Midi data (full line) and in the Sacramento Peak data (dotted line).

In the Pic-du-Midi data, a strict selection of 120 prominences out of 256 ones has been done in order to eliminate the geometrical errors; then, for all individual measurements the weights have been determined according to photometric accuracy only. In the Sacramento Peak data, the geometrical errors cannot be discarded in the same way, owing to the smaller size of the prominence sample; it is then not realistic to weigh each prominence, in which geometrical errors can occur, according to the number of averaged measurements  $w = \nu$ ; on the other hand, it would not be statistically fair to give the same weight  $w = 1$  to all the prominences because in some of them one measurement only has been done, for which photometric uncertainty is likely. As a compromise, we have used the values  $w \sim \sqrt{\nu}$  listed in Table 1 as weights in the least-square fitting of the Sacramento Peak data. However, the least-square fittings with  $w = 1$  and  $w = \nu$  have also been done, and have given the same minimum  $\alpha_m \sim -30^\circ$  for the squared residues  $(O - C)^2$  as the fitting given on Fig. 3.

The most probable value  $\alpha_m \sim -30^\circ$ , which is obtained as the result of the fitting, corresponds to the non-potential orientation of the prominence magnetic field with respect to the polarity of the neighbouring photospheric field. The good agreement which can be seen on Fig. 3 between the fits in the two sets of data shows that the same trend can be found in the two sets of prominences observed by the two instruments. However, the large size of the Pic-du-Midi sample of prominences has enabled more detailed analysis which have given evidence to two types of prominences (Leroy et al., 1984):

1) Prominences with maximum height larger than  $\sim 30\,000$  km. Their magnetic structure is consistent with the Kupcrus-Raadu type of models (i.e. non-potential sense of the prominence field). The mean  $\alpha$  value is  $\sim 25^\circ$  and the mean field strength is  $\sim 5$  to 10 Gauss. These prominences often show filamentary or curtain-like structures. Polar Crown prominences fall in this category.

2) Prominences with maximum height lower than  $\sim 30\,000$  km; their magnetic structure is consistent with the Kippenhahn-Schlüter type of model (i.e. potential sense of prominence field). The mean  $\alpha$  value is  $\sim 20^\circ$  and the mean strength is  $\sim 20$  Gauss. These prominences are bright, often sharp-edged in He I  $D_3$  and found essentially at low latitude.

These statistical results have been confirmed on favourable individual cases: for 15 prominences observed at Pic-du-Midi, the two-field vectors are pointing on the same side of the prominence, and the  $\alpha$  angles are large enough with respect to the measurements and interpretation inaccuracies, so that the field polarity is derived without any ambiguity.

#### References

- Athay, R. G., Querfeld, C. W., Smartt, R. N., Landi degl'Innocenti, E., Bommier, V.: 1983, *Solar Phys.*, **89**, 3.  
 Bommier, V., Leroy, J. L., Sahal-Bréchet, S.: 1981, *Astron. Astrophys.*, **100**, 231.  
 Leroy, J. L., Bommier, V., Sahal-Bréchet, S.: 1983, *Solar Phys.*, **83**, 135.  
 Leroy, J. L., Bommier, V., Sahal-Bréchet, S.: 1984, *Astron. Astrophys.*, **131**, 33.  
 Leroy, J. L., Bommier, V., Sahal-Bréchet, S., to be published.

Table 1. Averaged values for 12 prominences observed at Sacramento Peak (Athay et al., 1983) of the prominence aspect angle AA and azimuth angle  $\phi^*$  and  $\phi_s^*$  of the two magnetic field solutions with respect to the prominence long axis. The angles AA,  $\phi^*$ ,  $\phi_s^*$  are respectively related to the angles  $\beta$ ,  $\alpha_F$ ,  $\alpha_V$  defined in Leroy et al. (1984).  $\nu$  is the averaged number of measurements.

Prominence	Position Angle	AA	$\beta$	$\phi^*$ , $\phi_s^*$	$\alpha_F$ , $\alpha_V$	$\nu$	$w \sim \sqrt{\nu}$
BN1 79/04/24	212	-50	-130	-177, -83	-3, -97	4	2
BN2 79/04/25	212	-60	-120	-159, -81	-21, -99	1	1
BN3 79/04/26	215	-75	-105	-159, -52	-21, -128	2	1
BS1 79/04/26	208	0	-180	+135, -135	+45, -45	3	2
BS2 79/04/27	209	-15	-165	+132, -102	+48, -78	1	1
C1 79/04/25	27	15	-165	-36, +6	-36, +6	1	1
C2 79/04/27	28	15	-165	-35, +5	-35, +5	1	1
D1 80/08/15	121	30	150	+80, -140	+100, -40	20	4
D2 80/08/15	114	30	150	+87, -147	+93, -33	46	7
D3 80/08/16	115	30	150	+94, -154	+86, -26	19	4
E 80/09/17	262	45	135	+89, -179	+91, -1	1	1
F1 80/09/17	355	-10	-10	+70, -50	+70, -50	4	2
F2 80/09/19	355	-10	-10	+46, -26	+46, -26	25	5
GS 80/09/19	50	-40	140	-27, +107	-27, +107	13	4
GN 80/09/20	45	10	10	+21, -41	+21, -41	11	3
H 80/09/20	40	40	-140	-138, +58	-138, +58	12	3
I 80/10/18	115	70	110	+7, -147	+173, -33	9	3
L 80/10/22	115	70	110	-15, -125	-165, -55	11	3
M 80/10/22	250	40	-40	-177, +97	-3, +83	2	1